> PJ-015200-2024 <

Cryophotonics: Experimental Validation of a SOA model down to cryogenic temperatures

Maeva Franco, Lydia Kacel, Edwin Fontenelle, Pascal Morel, Thierry Rampone, Arnaud Gardelein and Ammar Sharaiha

***Abstract*— Cryophotonics is a promising way of boosting state-of-the-art photonic components using cryogenic temperatures. In this work, in addition to confirm our experimental results with measurements on another component, we present a theoretical analysis of SOA behavior at cryogenic temperatures. Based on the obtained experimental results, we expand the SOA model range by introducing temperature dependence on the main SOA physical parameters such as band gap energy level, recombination coefficients, internal losses and effective electron and holes masses. The model is applicable over a wide temperature range from ambient down to cryogenic temperatures. A qualitative agreement is found between simulations and experiments. The comparisons are given down to 70 K in terms of gain spectrum, saturation output power and noise figure which demonstrate the effectiveness of the model.**

***Index Terms*—Cryophotonics, Semiconductor Optical Amplifier, Temperature-dependent model.**

I. Introduction

Semiconductor optical amplifiers (SOA) are of great interest due to their integrability, their multi-band amplification possibility and their multi-functionality [1] [2]. New SOA designs or configurations are bringing improved performances in terms of optical bandwidth, noise figure and output power [3] [4] [5] [6] [7] [8] [9]. Recently, our team demonstrated that operating a SOA at cryogenic temperatures dramatically improves its performances in terms of gain level, noise figure and output power at low bias currents [10]. For instance, in comparison to room temperature, the chip gain is improved by 15 dB, the noise figure tends towards the theoretical limit of 3 dB and the saturation power is 2.5 dB higher. Thus, we showed that a cryogenic environment for SOA is a way to boost some system amplification parameters.

Modeling the SOA involves resolving the two coupled equations related to the carrier density rate and to the optical propagation fields. Simulations exploit the model by analyzing the SOA behavior as a function of bias current, optical input power and wavelength. Two main approaches of modeling SOA internal gain are used: phenomenological or physical. The former uses a linear, parabolic or cubic gain description [11] [12] [13] [14] [15]. The latter uses a physical approach [16] [17] [18] where modeling the material gain implies describing the physical process. Several papers [19] [20] have modeled the SOA as a function of the temperature using the SOA physical approach proposed by M. J. Connelly [17]. However, the temperature covered is close to room temperature, i.e. from -10°C to +60°C. Therefore, it is necessary to extend this model to enable accurate simulations over a wide range of temperatures, down to cryogenic temperatures. Hence the physical parameters controlling the model behavior must include temperature dependence.

In this paper, temperature-dependent modeling of SOA is presented alongside with a comparison between simulation and experimental results of the SOA system performances in terms of gain, saturation output power and noise figure. We present the experimental results concerning the Aeon's SOA referenced 64P37E which give similar behavior at cryogenic temperatures as in the first work that used another commercial SOA [10]. This SOA has been customized, replacing the thermo-electric cooler by a metal slab to have a better control of the chip temperature.

Having a fully quantitative model is complex, thus, as a first approach, we focus on obtaining a qualitative agreement between simulation and experimental results. For that, we consider the SOA modeling parameters given by M. J. Connelly in [17] representing a standard SOA not fitted to the one used in our measurements. We propose to modify the modeling parameters from [17] to take into account a broad temperature operating range.

In section II, we present the base SOA rate and propagation equations, detailing the physical terms that must contain temperature dependence. We show in section III the experimental behavior of the spectral response of the amplified spontaneous emission power and the gain of the used SOA. These behaviors state the experimental temperature dependence that a SOA model should be able to reproduce. In section IV, we present the physical terms that need to be expressed as a function of temperature in order to have similar behavior between simulation and experimental results. We detail their influence on the full SOA model temperature-related behavior. Section V is dedicated to assess the ability of our extended model to reproduce experimental system-level properties of the SOA, such as the gain, the saturation output power and the noise

Maeva Franco was previously with the Lab-STICC, CNRS UMR 6285, Plouzané, France and now with CROMA, CNRS UMR 5130, Grenoble, France (e-mail : maeva.franco@grenoble-inp.fr). Pascal Morel, Thierry Rampone and Ammar Sharaiha are with the Lab-STICC, CNRS UMR 6285, Plouzané, France (respective e-mails: morel@enib.fr, rampone@enib.fr, sharaiha@enib.fr).

Lydia Kacel and Edwin Fontenelle were internship students from the Lab-STICC, CNRS UMR 6285, Plouzané, France.

Arnaud Gardelein is with Air Liquide Advanced Technologies, Sassenage, France (e-mail: arnaud.gardelein@airliquide.com).

Authors would like to thank their financial supports being ESA contract 4000135867/21/NL/GLC/ov, CIFRE 2020/0779, Conseil Départemental du Finistère and Brest Métropole.

figure over a broad temperature range, down to cryogenic temperatures. Finally, the main results are summarized and perspectives are drawn.

II. SOA Generic Modeling Equations

The SOA is modeled and implemented following our previous work [12] where temperature dependence was not considered. The SOA is divided into sections along the propagation direction. The rate equation governing the carrier density evolution in the i[th] section is given by [12] [13] [17]:

$$\frac{dn_\mathrm{i}}{dt} = \frac{I_\mathrm{i}}{qwdL_\mathrm{i}} - R_\mathrm{i}^{nst}(n_\mathrm{i}) - R_\mathrm{i}^{ASE}(n_\mathrm{i}) - R_\mathrm{i}^{sig}(n_\mathrm{i}) \qquad (1)$$

where I_i is the bias current injected in the section i of the SOA (the total SOA current I_{bias} is the sum of all I_i) and L_i the length of this section. w is the width of the active zone of the SOA and d its depth. q is the elementary electric charge. R_i^{sig} states for the stimulated recombination rate due to the amplification of the optical signals and R_i^{ASE} for the recombination rate due to the amplified spontaneous emission (ASE). R_i^{nst}, the non-stimulated recombination rate, is given by [12] [13] [17]:

$$R_\mathrm{i}^{nst}(n_\mathrm{i}) = An_\mathrm{i} + B_{rad}{n_\mathrm{i}}^2 + C_{aug}{n_\mathrm{i}}^3 \qquad (2)$$

where $A = A_{rad} + A_{nrad}$, B_{rad} and C_{aug} are respectively the Shockley-Read-Hall (SRH), bimolecular and Auger recombination coefficients respectively.

In each section we consider the propagation of the envelop of the optical field as [12] [13] [17]:

$$F^{\pm}(z) = e^{\mp jk(n_\mathrm{i},\lambda)z}F^{\pm}(0) \qquad (3)$$

where k is the propagation constant defined by $k(n_\mathrm{i},\lambda) = \frac{2\pi n_e(n_\mathrm{i},\lambda)}{\lambda} + j\frac{g_n(n_\mathrm{i},\lambda)}{2}$. $n_e(n_\mathrm{i},\lambda)$ and $g_n(n_\mathrm{i},\lambda)$ are respectively the effective optical index and the net gain in SOA section i. It should be noted that ASE is considered as an intensity in the model.

Equations (1) to (3) define a generic set of equations where every parameter should be considered as temperature-dependent. In order to introduce temperature-dependent behaviors, we need to specify the temperature dependence of every term in these equations. In (1), some temperature-dependent terms are not explicit. Both $R_\mathrm{i}^{ASE}(n_\mathrm{i})$ and $R_\mathrm{i}^{sig}(n_\mathrm{i})$ depend on material gain and net gain which depend on temperature. In (2), A, B_{rad} and C_{aug} are temperature-dependent and explicit expression should be given. In (3), here again the temperature dependence is hidden in the optical index and net gain of the SOA. Section IV will be dedicated to introduce all the necessary temperature dependencies, except for the optical index for which we do not have measurements.

III. ASE and Gain Experimental Behavior at Cryogenic Temperatures

In this section we give an excerpt of the measured SOA response that will be taken as references for the model. In fact, our goal is to provide a model able to reproduce both ASE and amplification behaviors as a function of the temperature. The measured spectral response of the amplified spontaneous emission power P_{ASE} at several temperatures and 50 mA bias current is given in Fig. 1. In Fig. 2, we give the experimental results of the SOA optical chip gain G at 50 mA over a wide wavelength range up to gain transparency wavelengths. The SOA chip gain is calculated from the measured fiber-to-fiber gain and adding estimated coupling losses, as described in [10]. The inset in Fig. 2 is a close-up view of the transparency regime, corresponding to the flat part of the spectra. It is reached when the material gain is null because the photon energy falls inside the band gap meaning that the gain only contains losses term at these wavelengths.

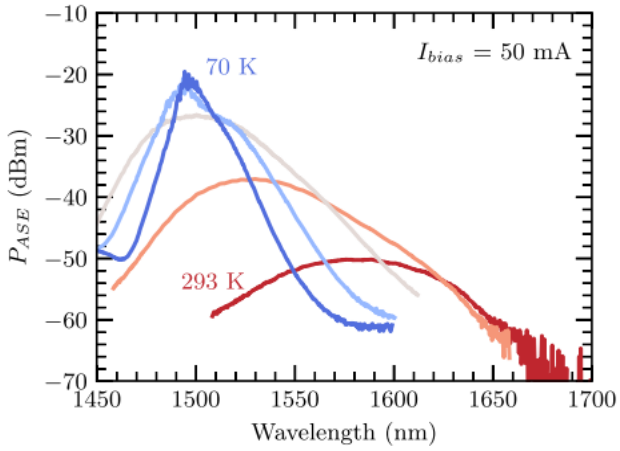

Fig. 1. Experimental ASE spectra at a bias current of 50 mA. The temperatures are 293 K, 240 K, 180 K, 120 K and 70 K from dark red to dark blue. This measure is obtained at the Optical Spectrum Analyzer with a 100 pm resolution.

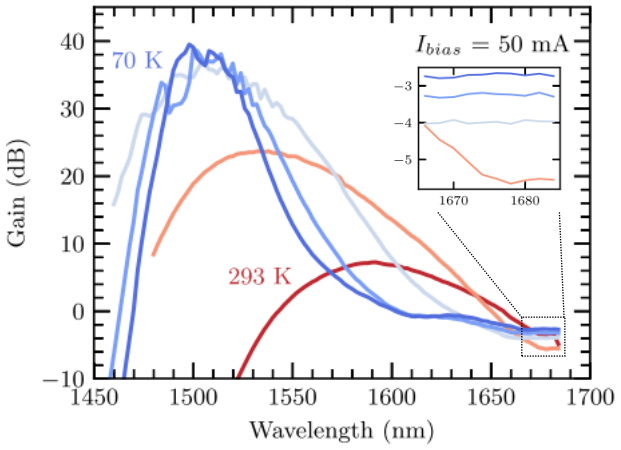

Fig. 2. Experimental SOA chip gain spectra at a bias current of 50 mA. The temperatures are 293 K, 240 K, 180 K, 120 K and 70 K from dark red to dark blue. The inset corresponds to the gain focusing at transparency wavelengths.

In Fig. 1 and 2, we observe that both ASE and gain spectra shift towards shorter wavelengths as the temperature lowers.

Their level increases while their optical bandwidth decreases. In addition, we observe that the SOA gain at the transparency regime increases with the temperature, confirming the reduction of α at cryogenic temperatures [16].

IV. Temperature Dependence of Material Gain, Gain Coefficient and Internal Losses

In order to introduce exhaustive temperature dependence down to cryogenic temperature, we have to work on the different parameters used in the generic system of equation presented in section II. A major parameter in SOAs is their net gain, given as $g_n = \Gamma g_m - \alpha$, where Γ is the confinement factor, g_m the material gain and α the internal losses. In our work we assume that the confinement factor is not considered as dependent on temperature because it is linked to the geometry of the active zone. The temperature dependence of α will be treated in section IV-C. Following [17], the material gain g_m is given as

$$g_m(n,\lambda,T) = g_0(n,\lambda)\sqrt{1-\frac{E_g(n)}{E_p}}\left(f_c(n,\lambda,T) - f_v(n,\lambda,T)\right) \quad (4)$$

where $g_0(n,\lambda)$, $E_g(n)$, $f_c(n,\lambda,T)$ and $f_v(n,\lambda,T)$ are defined in appendix 1 respectively by (A.1), (A.3), (A.4) and (A.5).

To state the interest of forthcoming model improvements, we show in Fig. 3 the SOA gain simulation results obtained by using [12] and [17]. The gain in dB is calculated as $10\ \log(e^{g_n L})$ where L is the SOA active zone length given in table I in appendix 2. We call this obtained starting model as "room-temperature model" (RT model) in following discussion.

The simulated gain spectrum is dependent on the temperature. However, its evolution does not match at all the SOA behavior observed experimentally (see Fig. 1 and 2): the wavelength shift is weak, the optical bandwidth does not reduce and the transparency gain does not tend towards 0.

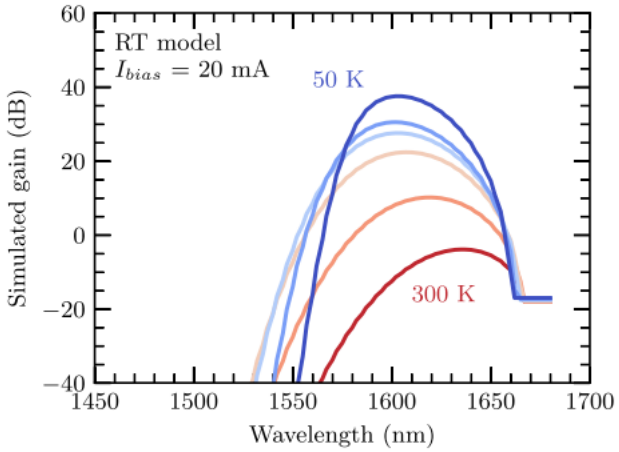

Fig. 3. Step 0, gain spectra as a function of the temperature using the room-temperature model [12] [17] [11,17]. The temperature evolves from 300 K (dark red) to 50 K (dark blue) with a 50 K temperature step.

It should be noted that we set in simulation the SOA bias current I_{bias} at 20 mA and compare the obtained results with the experimental ones at 50 mA. For these I_{bias} settings, the simulation and the experimental results will finally give a similar qualitative behavior once all temperature dependencies are well taken into account.

In order for the SOA model to match the experimental behavior, we introduce the temperature dependence in all the terms of (2) and (4).

In the following we will gradually show the influence of each term on the SOA gain spectra.

A. Temperature dependence of the band gap

A critical term in the material gain model is of course the band gap. To take into account its variation with respect to temperature, one has to use Varshini's model [21] as follows:

$$E_g(n,T) = E_g(n) - E_g(T) \quad (5)$$

$$E_g(T) = \frac{b_T T^2}{T + a_T} \quad (6)$$

where, a_T and b_T are constants depending on the SOA chip material.

Fig. 4 shows the simulated SOA gain as a function of the temperature by introducing $E_g(n,T)$. We observe that the SOA gain spectrum notably shifts towards lower wavelengths by reducing the temperature.

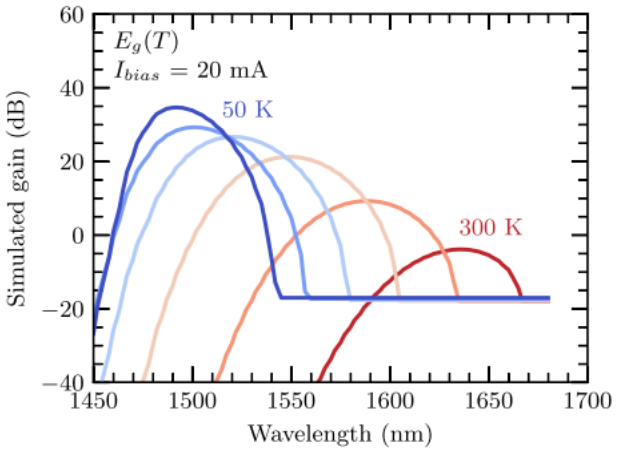

Fig. 4. Step 1, contribution of the temperature-dependent band gap energy model given in [21]. The temperature evolves from 300 K (dark red) to 50 K (dark blue) with a 50 K temperature step.

B. Temperature dependence of recombination coefficients and effective electron and hole masses

1) Recombination coefficients

In semiconductors, A_{rad} and C_{aug} generally decrease when the temperature decreases while B_{rad} increases strongly [22] [23] [23-24].

The basic temperature-dependent model for A_{rad} follows the usual power-law relationship [24]:

$$A_{rad}(T) = A_{rad}(T_{ref})\left(\frac{T}{T_{ref}}\right)^{\eta} \quad (7)$$

where $A_{rad}(T_{ref})$ is the A_{rad} coefficient at room temperature and $\eta = 1.77$ as in [23].

B_{rad} temperature dependence is described as an inverse law of the form $\left(\frac{1}{T}\right)^{\delta}$ where the exponent δ is between 1 and 1.5 [23-24]. Here we use for $B_{rad}(T)$ the following expression with $\delta = \frac{3}{2}$ [23]:

$$B_{rad}(T) = B_{rad}(T_{ref}) \left(\frac{T_{ref}}{T}\right)^{3/2} \quad (8)$$

where $B_{rad}(T_{ref})$ is the B_{rad} coefficient at room temperature.

The relationship for the Auger process at different temperatures is also given by [23]:

$$C_{aug}(T) = C_{aug}(T_{ref}) e^{-\frac{E_c}{kT}} \quad (9)$$

where $C_{aug}(T_{ref})$ is the Auger coefficient at room temperature and E_c is the Auger activation energy having a value of 4.3 meV [23].

2) Effective electrons and holes masses

The effective mass of electrons m_e, heavy holes m_{hh} and light holes m_{lh} are temperature-dependent [25]. Their respective developments depend on the value of the energy of the band gap which itself depends on the temperature. The expressions of masses are given by the following equation [25]:

$$m_{e/lh/hh}(T) = m_{e/lh/hh}(T_{ref}) \frac{E_g(n,T_{ref})}{E_g(n,T)} \quad (10)$$

where T_{ref} is the room-temperature and $m_{e/lh/hh}$ stands for m_e, m_{lh} or m_{hh}.

3) Simulation results

Fig. 5 shows the contribution of $E_g(n,T)$ and the radiative recombination coefficient $B_{rad}(T)$. We observe that in addition to the shift of the SOA gain spectrum due to $E_g(n,T)$, a reduction of the optical bandwidth takes place as the temperature decreases. A more detailed explanation is given later in this section about the influence of B_{rad} parameter on the optical gain bandwidth.

We can see the contribution of $A_{rad}(T)$ and $C_{aug}(T)$ in Fig. 6 and the one of $m_{e,lh,hh}(T)$ in Fig. 7.

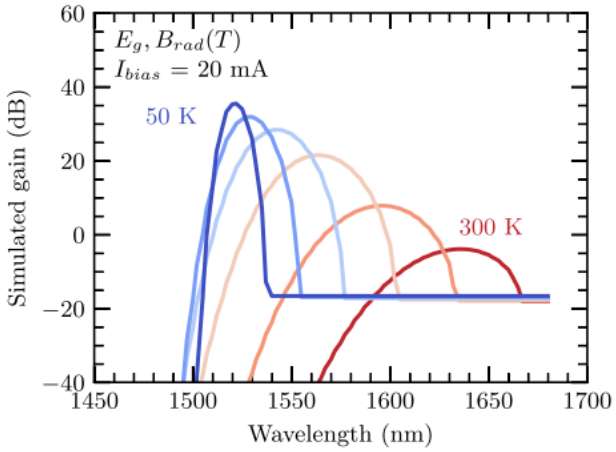

Fig. 5. Step 2, added contribution of $B_{rad}(T)$ [23]. The temperature evolves from 300 K (dark red) to 50 K (dark blue) with a 50 K temperature step.

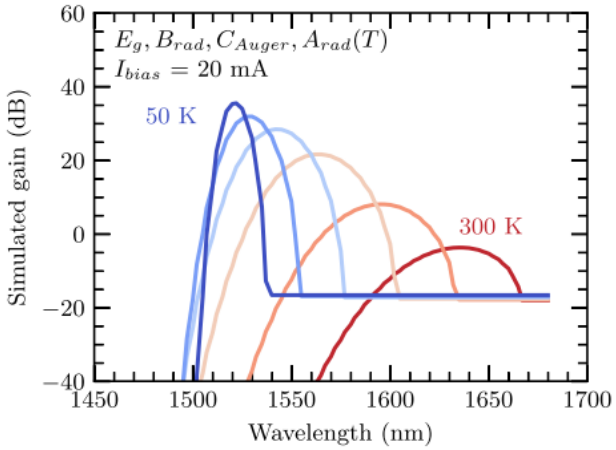

Fig. 6. Step 3, added contribution of $A_{rad}(T)$ and $C_{Auger}(T)$ [23]. The temperature evolves from 300 K (dark red) to 50 K (dark blue) with a 50 K temperature step.

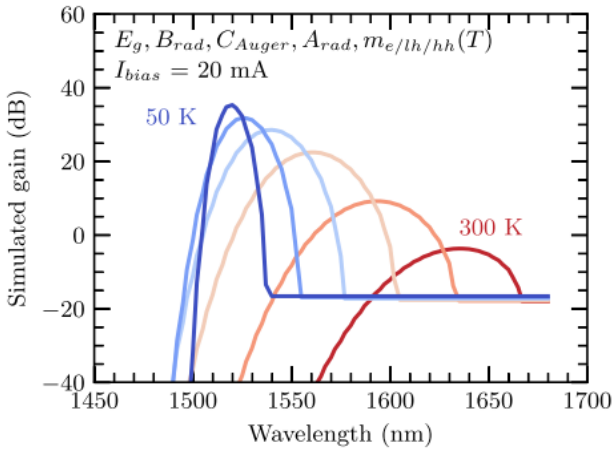

Fig. 7. Step 4, added contribution of the effective masses [25]. The temperature evolves from 300 K (dark red) to 50 K (dark blue) with a 50 K temperature step.

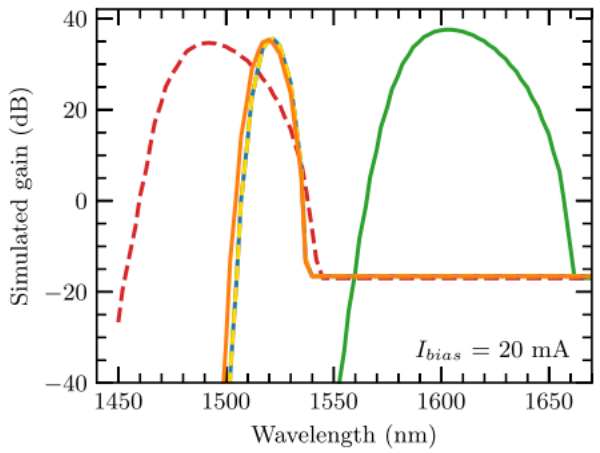

Fig. 8. Evolution of the simulated gain at 50 K when adding the different contributions. Solid green: room-temperature model (step 0). Dotted red: contribution of the bandgap (step 1). Solid blue: contribution of the radiative recombination coefficient $B_{rad}(T)$ (step 2). Dotted yellow: contribution of the recombination coefficient $A_{rad}(T)$ and the Auger recombination coefficient $C_{aug}(T)$ (step 3). Solid orange: contribution of the effective masses $m_{e,lh,hh}(T)$ (step 4).

To better illustrate the associated behavior of each term, we summarized in Fig. 8 the evolution of the different contributions at 50 K. One can see that the main contributors are the band gap energy for the wavelength shift and the radiative recombination coefficient $B_{rad}(T)$ for the bandwidth shrinking. The contribution of the radiative coefficient $A_{rad}(T)$ and $C_{aug}(T)$is not significant (solid blue and dotted yellow line) and the contribution of the effective masses is very small.

We will now focus on the optical amplification bandwidth. To explain its behavior as a function of the different model parameters, we must recall that the optical amplification bandwidth at -3 dB from the peak gain is function of the energy interval ΔE_B of the amplification regime for a photon of energy $E_p = \frac{hc}{\lambda}$. To be amplified, an input signal must be between transparency and absorption regimes which can be expressed by: $E_g(n,T) < E_p < E_{fc}(n,T) - E_{fv}(n,T) + E_g(n,T)$. $E_{fc}(n,T)$ is the quasi-Fermi level of the conduction band (CB) relative to the bottom of the conduction band and $E_{fv}(n,T)$ is the quasi-Fermi level of the valence band (VB) relative to the top of the valence band. ΔE_B can be given from (A.8) and (A.9) by:

$$\Delta E_B = E_{fc}(n,T) - E_{fv}(n,T) = kT\left(\left(\ln(\delta) + \frac{\delta}{\left(64+0.05524\delta\left(64+\sqrt{\delta}\right)\right)^{1/4}}\right) + \left(\ln(\varepsilon) + \frac{\varepsilon}{\left(64+0.05524\varepsilon\left(64+\sqrt{\varepsilon}\right)\right)^{1/4}}\right)\right) \quad (11)$$

where δ and ε are in function of carrier density (cf. Appendix).

Figure 9 shows the simulated evolution of the carrier density (n_{avg}) corresponding to the averaged carrier density over the M sections as $n_{avg} = \frac{\sum n_i}{M}$. In Fig. 9, different cases are considered: for the RT model, for the RT model to which we add the temperature dependency of E_g and finally the RT model to which we add the temperature dependency of E_g and B_{rad}. We observe that in the last case the decrease of the carrier density by lowering the temperature is more important, showing the influence of B_{rad}. This contributes to a reduction of the gain optical bandwidth as shown in Fig. 5, in better agreement with the experimental results in Fig. 2.

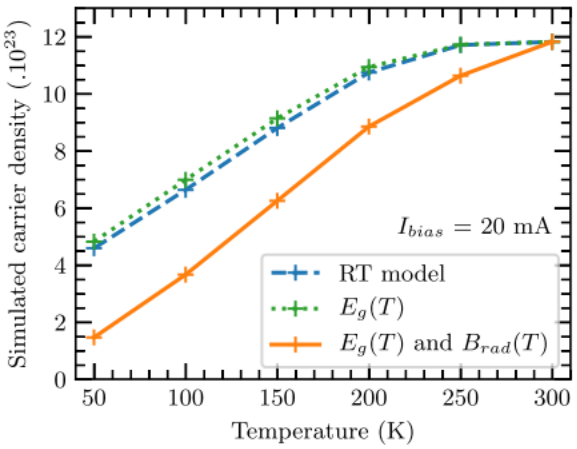

Fig. 9. Evolution of the carrier density n_{avg} as a function of the temperature using the room-temperature model (dashed line), using the temperature dependence on the term E_g (dotted line) and using the temperature dependence on both E_g and B_{rad} (full line).

C. Internal losses

In [17] the internal losses are expressed as

$$\alpha(n) = k_0 + k_1 n \quad (12)$$

where k_0 is the carrier-independent absorption losses coefficient and k_1 is the carrier-dependent absorption losses coefficient.

To take into account the temperature dependence of the internal losses, we have to follow [16] where the losses are described as $\alpha(n,T) = \alpha_1(n,T) + \alpha_2(n,T)$ where:

$$\alpha_1 = \frac{B_1}{1+\exp\left(\frac{E_1 - E_{fv}}{k_B T}\right)} \quad (13)$$

$$\alpha_2 = \frac{B_2}{1+\frac{1}{2}\exp\left(\frac{E_A - E_{fv}}{k_B T}\right)} \quad (14)$$

B_1 and B_2 are constants defined so as to fit the best the experimental results, E_1 and E_A are energy levels, E_{fv} is the Fermi quasi-level of the valence band and k_B is the Boltzmann

constant.

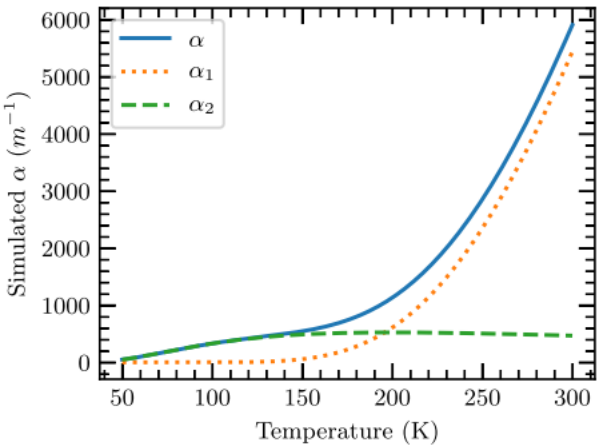

Fig. 11. Evolution of the simulated internal losses as a function of the temperature [16].

Fig. 11 presents the evolution of the internal losses as a function of the temperature. One can see that at room temperature α_1 is the major contributor while under 200 K α_2 dominates. In all cases the internal losses decrease when the temperature lowers. This is why in Fig. 2, one can see the transparency level moving towards 0 dB when the temperature lowers.

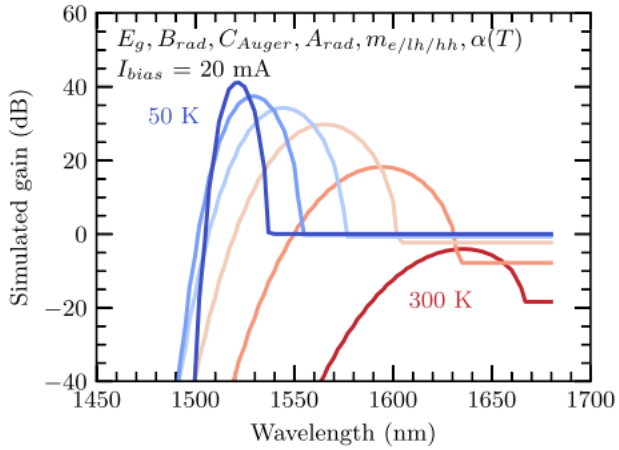

Fig. 12. Step 5, addition of the influence of the internal losses. The temperature evolves from 300 K (dark red) to 50 K (dark blue) with a 50 K temperature step.

Fig. 12 shows the simulation result of the gain when all temperature-dependent terms are considered. As in the experimental gain in Fig. 2, we can see the influence on the internal losses at the transparency regime. However, the obtained gain spectrum shift in Fig. 12 does not slow down as much as in the experimental results when the temperature lowers. In Fig. 2, we can notice in particular that the shift tends to stabilize at lower temperatures. In addition, the level of α is lower at the transparency regime. This can be adjusted by changing the temperature parameters of E_g and α. For example, with $b_T = 1.25$, $B_1 = 2520$ and $B_2 = 0.56 \times 10^7$, the gain spectrum presents better concordance with the experimental one in Fig. 2 as shown in Fig. 13.

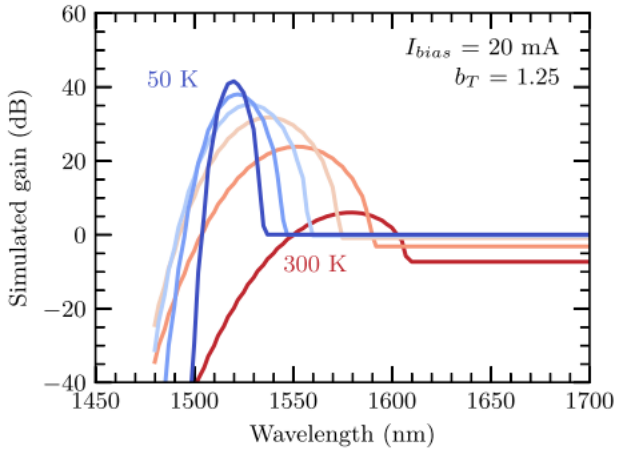

Fig. 13. Simulated gain spectrum as a function of the temperature with the coefficients $b_T = 1.25$, $B_1 = 2520$ and $B_2 = 0.56 \times 10^7$. The temperature evolves from 300 K (dark red) to 50 K (dark blue) with a 50 K temperature step.

The model is also applicable to simulate the evolution of the amplified spontaneous emission power P_{ASE}. Figure 14 shows the evolution of P_{ASE} which is good agreement with the experimental results as shown in Fig. 1.

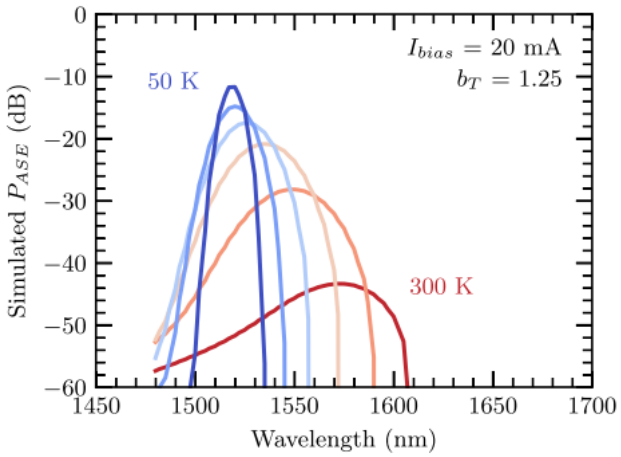

Fig. 14. Simulated ASE spectrum as a function of the temperature. The temperature evolves from 300 K (dark red) to 50 K (dark blue) with a 50 K temperature step.

V. Output Saturation Power and Noise Figure at Cryogenic Temperature

As presented experimentally [10], we have shown improved system performances at low temperature, such as higher output saturation power (P_{-3dB}) and lower noise figure (NF). In the following, we present the experimental results of the Aeon's SOA and the simulation responses for the output saturation power P_{-3dB} and the noise figure NF. As mentioned before, we use a standard SOA model not fitted to the one used in our measurements such that only a qualitative comparison can be done between experimental and simulated behaviors. This is the main reason for the observed differences in the following between measured and simulated P_{-3dB} and NF values.

A. Output saturation power

The output saturation power P_{-3dB} is the output power for which the SOA gain decreases by 3 dB. The experimental results of P_{-3dB} are obtained by varying the input power following the peak gain wavelength. It is enhanced at low temperature (Fig. 15) similar to the behavior observed in [10].

In Fig. 16, the simulation result shows that the saturation power at -3 dB increases as the temperature lowers.

The increase of P_{-3dB} at low temperature can be related to two physical parameters of the SOA: the gain coefficient $\frac{dg_m}{dn}$ and the effective carrier lifetime τ_{eff} [26] [27] [28] [26-28]. To calculate this parameter, we calculate $\frac{dg_m}{dn}$ using the carrier density average value over all sections. Similarly, we calculate τ_{eff} as the average value of the effective carrier lifetime in all sections. The effective carrier lifetime in section i is given by

$$\tau_{eff}(\mathrm{i}) = \frac{n_\mathrm{i}}{\left(R_\mathrm{i}^{nst}(n_\mathrm{i}) + \mathrm{R}_\mathrm{i}^{ASE}(n_\mathrm{i})\right)} \tag{15}$$

The relationship between P_{-3dB}, $\frac{dg_m}{dn}$ and τ_{eff} is given by [29]:

$$P_{-3dB} \sim \ln(2) P_{sat} \tag{16}$$

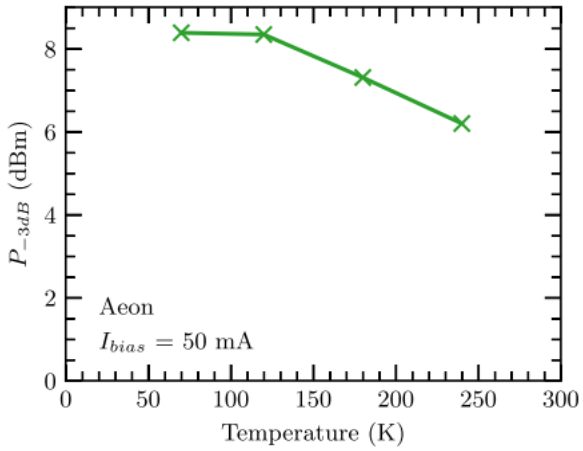

Fig. 15. Experimental evolution of the output saturation power as a function of the temperature.

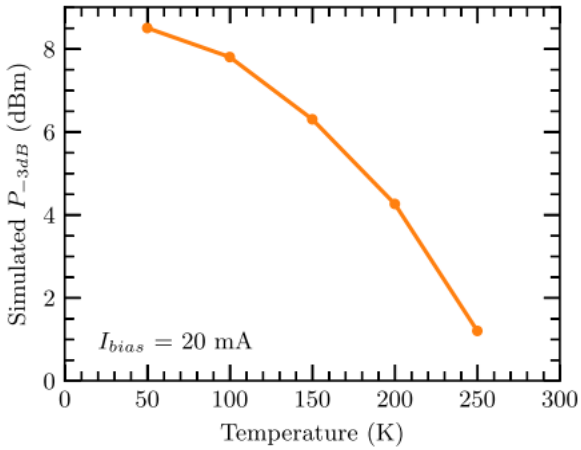

Fig. 16. Simulation of the output saturation power as a function of the temperature.

with

$$P_{sat} = \frac{h\nu wd}{\Gamma \frac{dg_m}{dn} \tau_{eff}} \tag{17}$$

The variation of the gain coefficient $\frac{dg_m}{dn}$ and τ_{eff} as a function of temperature is shown in Fig. 17. It is obtained by modeling coarsely the SOA with only one calculation section. This figure also shows the variation of both parameters in two opposite directions. The gain coefficient $\frac{dg_m}{dn}$ increases slightly by lowering the temperature and thus tends to reduce P_{-3dB} while τ_{eff} decreases highly (by a factor of about 12.5 at 20 mA), compared to $\frac{dg_m}{dn}$, which assists P_{-3dB} to increase. Thus, the product $\frac{dg_m}{dn}.\tau_{eff}$ in (17) decreases continuously allowing P_{-3dB} to enhance at cryogenic temperatures.

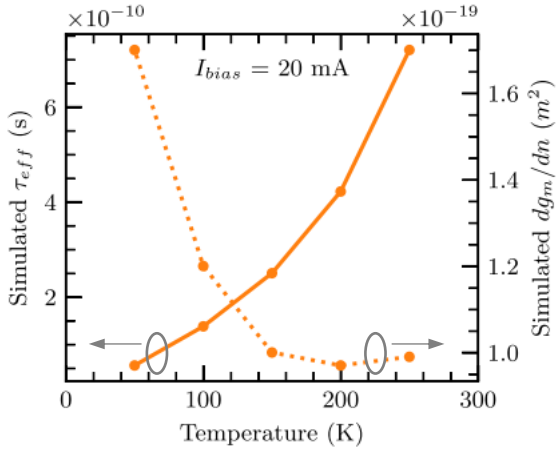

Fig. 17. Evolution of the simulated effective carrier lifetime (solid line) and the gain coefficient (dotted line) as a function of the temperature at 20 mA.

B. Noise figure

The noise figure is calculated following the peak gain wavelength as in [7]. The noise figure is evaluated without taking into account coupling losses. The obtained result show that the NF of the SOA decreases at low temperatures (Fig. 18). At 50 mA, the NF tends towards 4 dB approaching the theoretical limit of 3 dB.

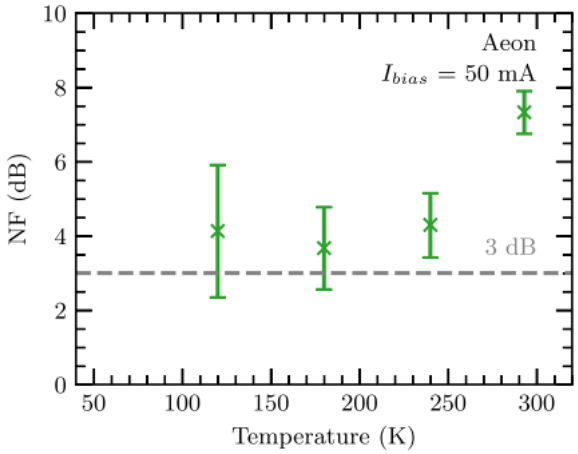

Fig. 18. Noise figure as a function of the temperature at 50 mA.

The NF simulation results in Fig. 19 present a behavior in good agreement with Fig. 18, showing a decrease of the NF at low temperatures.

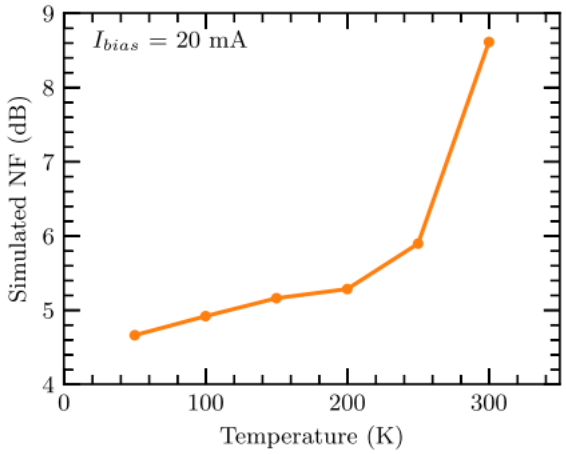

Fig. 19. Evolution of the simulated noise figure as a function of the temperature at 20 mA.

The NF decrease can be explained by relying on the theoretical NF definition given by [30]:

$$NF = 3 + 10\log\left(\frac{\Gamma g_m}{\Gamma g_m - \alpha}\right) + 10\log(n_{sp}) \quad (18)$$

where n_{sp} is the population inversion factor calculated as:

$$n_{sp} = \left(1 - \exp\left(\frac{E_p - \Delta E_B}{k_B T}\right)\right)^{-1} \quad (19)$$

In fact, (18) shows that the NF decreases due to two terms: the internal losses α and the population inversion factor n_{sp}. α becomes negligible at cryogenic temperatures (Fig. 10 and 12) and n_{sp} decreases from 1.66 to 1.46 while cooling the SOA from 200 K to 50 K.

VI. Conclusion

In a previous work we have reported how cryogenic environment dramatically improves Semiconductor Optical Amplifier performances. Modeling the behavior is a key to understand the origin of the performance improvement. To the best of our knowledge, current models can only be used close to room-temperature. In this paper we develop a SOA extended model down to cryogenic temperatures based on the experimental results of SOA gain and ASE over the temperature range 293 K to 70 K. To achieve this goal, we first reproduced the experiment on another commercial SOA. In a second step, we gathered the results of several analytical studies to describe the temperature dependence of the physical parameters such as the band gap, the effective masses or the intrinsic losses and showed their influences on the SOA gain. Thus, the extended model allows us to qualitatively reproduce the observed behavior of the tested SOA. Moreover, we are able to better understand the evolution of other SOA characteristics as a function of the temperature such as SOA output saturation power and noise figure. For instance, we demonstrated that the noise figure actually tends towards the theoretical limit of 3 dB.

As a perspective to obtain a quantitative model, further investigations are required on physical parameters values to better fit the behavior of a given SOA.

The association of photonics with cryogenics opens new perspectives in domains such as optical communications or quantum computing. With this model we pave the way for future development in cryophotonics.

Appendix 1

Here we define the terms present in the material gain definitions cited in (4) and (5). The equations are given in M. J. Connelly's model [17].

$$g_0(n,\lambda) = \frac{\lambda^{3/2}\sqrt{c}}{4\sqrt{2}\pi^{\frac{3}{2}} n_e^2 \tau(n)} m_f \quad (A.1)$$

where c is the speed of light in vacuum, n_e is the refractive index in the active region, and m_f is dependent of the masses as $m_f = \left(\frac{4\pi m_e m_{hh}}{h(m_e + m_{hh})}\right)^{3/2}$ where m_e and m_{hh} are respectively the electron mass in the conduction band (CB) and the heavy hole mass of the valence band (VB).

The carrier lifetime $\tau(n)$ is function of the radiative recombination coefficients A_{rad} and B_{rad} following

$$\tau(n) = 1/(A_{rad} + B_{rad} n) \quad (A.2)$$

Equation (A.3) describes the bandgap energy:

$$E_g(n) = e(a + by + cy^2) - eK_g n^{1/3} \quad (A.3)$$

where a, b and c are the quadratic coefficients, y is the molar fraction of Arsenide in the SOA active region, e the electronic charge and K_g the bandgap shrinkage coefficient.

The Fermi-Dirac distributions $f_c(n,\lambda,T)$ and $f_v(n,\lambda,T)$ in the CB and VB are given by:

$$f_c(n,\lambda,T) = \frac{1}{1+\exp\left(\frac{E_a(n,\lambda,T) - E_{fc}(n,T)}{k_B T}\right)} \quad (A.4)$$

$$f_v(n,\lambda,T) = \frac{1}{1+\exp\left(\frac{E_b(n,\lambda,T) - E_{fv}(n,T)}{k_B T}\right)} \quad (A.5)$$

where,

$$E_a(n,\lambda,T) = \left(E_p - E_g(n)\right)\frac{m_{hh}}{(m_e + m_{hh})} \quad (A.6)$$

$$E_b(n,\lambda,T) = -\left(E_p - E_g(n)\right)\frac{m_e}{(m_e + m_{hh})} \quad (A.7)$$

T is the absolute temperature and k_B the Boltzmann constant. $E_{fc}(n,T)$ is the quasi-Fermi level of the CB relative to the

bottom of the band. $E_{fv}(n,T)$ is the quasi-Fermi level of the VB relative to the top of the band.

$$E_{fc}(n,T) = kT\left(\ln(\delta) + \frac{\delta}{\left(64+0.05524\delta(64+\sqrt{\delta})\right)^{1/4}}\right) \quad \text{(A.8)}$$

$$E_{fv}(n,T) = -kT\left(\ln(\varepsilon) + \frac{\varepsilon}{\left(64+0.05524\varepsilon(64+\sqrt{\varepsilon})\right)^{1/4}}\right) \quad \text{(A.9)}$$

with $\delta = \frac{n}{n_c}$, $n_c = 2\left(\frac{2\pi m_e kT}{h}\right)^{3/2}$ and $\varepsilon = \frac{p}{n_v}$. $n_v = 2\left(\frac{2\pi m_{dh} kT}{h}\right)^{3/2}$ where $m_{dh} = \left(m_{hh}^{3/2} + m_{lh}^{3/2}\right)^{2/3}$ with m_{lh} the effective mass of a light hole in the VB and p is the hole density in the VB.

APPENDIX 2

TABLE I
SIMULATION PARAMETERS

Symbol	Parameter	Value
L	Active zone length	600 µm
w	Active zone width	0.4 µm
d	Active zone depth	0.4 µm
Γ	Confinement factor	0.45
$a_{T_{ref}}$	Energy band constant coefficient	1.35
$b_{T_{ref}}$	Energy band linear coefficient	-0.775
$c_{T_{ref}}$	Energy band quadratic coefficient	0.149
y	Molar fraction of Arsenide	0.892
$A_{rad}(T_{ref})$	Linear radiative recombination coefficient	$1\text{x}10^{-7}$ s^{-1}
$B_{rad}(T_{ref})$	Bimolecular radiative recombination coefficient	$5.6\text{x}10^{-16}$ $m^3.s^{-1}$
$C_{Auger}(T_{ref})$	Auger recombination coefficient	$3\text{x}10^{-41}$ m^{-6} s^{-1}
T_{ref}	Reference temperature	300 K
k_0	Absorption losses coefficient	6200 m^{-1}
k_1	Carrier dependent absorption losses coefficient	$7500\text{x}10^{-24}$ m^{-4}
K_g	Energy band shrinking coefficient	$0.9\text{x}10^{10}$ eVm
n_e	Refractive index in the active region	3.22
$m_e(T_{ref})$	Effective mass of electrons in the conduction band	$4\text{x}10^{-32}$ kg
$m_{hh}(T_{ref})$	Effective mass of heavy holes in the valence band	$4.19\text{x}10^{-31}$ kg
$m_{lh}(T_{ref})$	Effective mass of light holes in the valence band	$5.06\text{x}10^{-32}$ kg

REFERENCES

[1] A. Sobhanan, A. Anthur, S. O'Duill, M. Pelusi, S. Namiki, L. Barry, D. Venkitesh and G. Agrawal, "Semiconductor optical amplifiers: recent advances and applications," *Advances in Optics and Photonics*, vol. 14, no. 3, pp. 571-651, 2022.

[2] H. Tang, C. Yang, L. Qin, L. Liang, Y. Lei, P. Jia, Y. Chen, Y. Wang, Y. Song, C. Qiu, C. Zheng, X. Li, D. Li and L. Wang, "A review of high-power semiconductor optical amplifiers in the 1550 nm band," *Sensors*, vol. 17, no. 7326, 2023.

[3] T. Motaweh, A. Sharaiha, L. Ghisa, P. Morel, M. Guégan, R. Brenot and A. Verdier, "Performing broadband optical transmission links by appropriate spectral combination of broadband SOA gain, Raman amplification and transmission fiber losses," *Optics communication*, vol. 385, pp. 66-70, 2017.

[4] J. Renaudier and et al., "Recent advances in 100+nm ultra-wideband fiber-optic transmission systems using semiconductor optical amplifiers," *Journal of Lightwave Technology*, vol. 38, no. 5, pp. 1071-1079, 2020.

[5] S. Yu, A. Gallet, I. Demirtzioglou, S. Azouigui, N. Dahdah and R. Brenot, "New SOA design with large gain, small noise figure, and high saturation output power level," *IEEE Journal of Quantum Electronics*, vol. 60, no. 2, pp. 1-7, 2024.

[6] J. Renaudier, C. Calo and A. Ghazisaeidi, "Towards >100Tb/s ultra wideband transmission systems," in *Proceedings of the 2022 Conference on Lasers and Electro-Optics Pacific Rim*, 2022.

[7] T. Briant, P. Grangier, R. Tualle-Brouri, A. Bellemain, R. Brenot and B. Thedrez, "Accurate determination of the noise figure of polarization-dependent optical amplifiers: theory and experiment," *Journal of Lightwave Technology*, vol. 24, no. 3, pp. 1499-1503, 2006.

[8] K. Carney, R. Lennox, R. Maldonado-Basilio, S. Philippe, F. Surre, L. Bradley and P. Landais, "3.8dB noise figure in bulk semiconductor optical amplifier," in *CLEO-PR*, Kyoto, 2013.

[9] C. Pham, F. Duport, R. Brenot, J.-F. Paret, A. Garreau, C. Gomez, C. Fortin, K. Mekhazni and F. van Dijk, "Modulation of a high power semiconductor optical amplifier for free space communications," *Journal of Lightwave Technoplogy*, vol. 38, no. 7, pp. 1836-1843, 2020.

[10] M. Franco, A. Gardelein, P. Morel and A. Sharaiha, "Towards cryophotonics: experimental characterization of SOA at cryogenic temperatures," *IEEE Photonics Journal*, vol. 15, no. 1, pp. 1-10, 2021.

[11] P. Morel, A. Sharaiha, R. Brenot and B. Thédrez, "Wideband gain and noise figure modeling in SOA," *Optical and Quantum Electronics*, vol. 38, pp. 231-236, 2006.

[12] P. Morel and A. Sharaiha, "Wideband time-domain transfer matrix model equivalent circuit for short pulse propagation in semiconductor optical amplifiers," *Optical and Quantum Electronics*, vol. 45, no. 2, pp. 103-116, 2009.

[13] T. Durhuus, B. Mikkelsen and K. Stubkjaer, "Detailed dynamic model for semiconductor optical amplifiers and their crosstalk and intermodulation distortion," *Journal of Lightwave Technology*, vol. 10, no. 8, pp. 1056-1065, 1992.

[14] G. Sartoris and J. Leuthold, "Modeling semiconductor optical devices," *Journal of Modeling and Simulation of Microsystems*, vol. 1, no. 1, pp. 1-8, 1999.

[15] J. Leuthold, M. Mayer, J. Eckner and G. Guekos, "Material gain of bulk 1.55 µm InGaAsP/InP semiconductor optical amplifiers approximated by a polynomial model," *Journal of Applied Physics*, vol. 87, no. 1, pp. 618-620, 2000.

[16] M. Asada and Y. Suematsu, "The effects of loss and nonradiative recombination on the temperature dependence of threshold current

in 1.5-1.6 µm GalnAsP/InP lasers," *IEEE Journal of Quantum Electronics*, vol. 19, no. 6, pp. 917-923, 1983.

[17] M. J. Connelly, "Wideband semiconductor optical amplifier steady-state numerical model," *IEEE Journal of Quantum Electronics*, vol. 37, no. 3, pp. 439-447, 2001.

[18] T. Motaweh, P. Morel, A. Sharaiha, R. Brenot, A. Verdier and M. Guégan, "Wideband gain MQW-SOA modeling and saturation power improvement in a tri-electrode configuration," *IEEE Journal of Lightwave Technology*, vol. 35, no. 10, pp. 2003-2009, 2017.

[19] Y. Kumar and M. R. Shenoy, "Enhancement in the gain recovery of a semiconductor optical amplifier by device temperature control," *Pramana*, vol. 87, no. 82, pp. 1-6, 2016.

[20] R. M. Ibrahim, I. B. Karomi, O. F. Ameen and M. S. Al-Ghambi, "Temperature-dependency performance of InGaAsP semiconductor laser amplifiers," *Digest Journal of Nanomaterials and Biostructures*, vol. 16, no. 2, pp. 385-392, 2021.

[21] Y. P. Varshini, "Temperature dependence of the energy gap in semiconductors," *Physica*, vol. 34, pp. 149-154, 1967.

[22] H.-Y. Ryu, G.-H. Ryu, C. Onwukaeme and B. Ma, "Temperature dependence of the Auger recombination coefficient in InGaN/GaN multiple-quantum-well light-emitting diodes," *Optics Express*, vol. 28, no. 19, pp. 27459-27472, 2020.

[23] P. Prajoon, D. Nirmal, M. A. Menokey and J. C. Pravin, "Temperature-dependent efficiency droop analysis of InGaN MQW light-emitting diode with modified ABC model," *Journal of Computational Electronics*, vol. 15, no. 4, pp. 1511-1520, 2016.

[24] D. B. M. Klaassen, "A unified mobility model for device simulation- II. Temperature dependence of carrier mobility and lifetime," *Solid-State Electronics*, vol. 35, no. 7, pp. 961-967, 1992.

[25] V. Gopal, "Temperature dependence of effective mass of electrons & holes and intrinsic concentration in silicon," *Indian Journal of Pure and Applied Physics*, vol. 20, pp. 180-182, 1982.

[26] P. Baveja, A. Kaplan, D. Maywar and G. Agrawal, "Pulse amplification in semiconductopr optical amplifiers with ultrafast gain-recovery times," in *Proc. SPIE*, 2010.

[27] V. Agrawal and M. Agrawal, "Characterization and optimization of semiconductor optical amplifier for ultra high speed applications: A review," in *SPACES*, Vijayawada, India, 2018.

[28] N. Hamdash, A. Sharaiha, T. Rampone, D. Le Berre, N. Martin and C. Quendo, "Small-signal analysis in two calculation sections and experimental validation of up-converted coherent population oscillations in semiconductor optical amplifiers," *IEEE Photonics Journal*, vol. 13, no. 4, pp. 1-10, 2021.

[29] Y. Yamamoto, Coherence, amplification and quantum effects in semiconductor lasers, Wiley-Interscience, 1991, p. 646.

[30] S. Yu, A. Gallet, N. El Dahdah, H. Elfaiki, I. Demirtzioglou, L. Godard and R. Brenot, "Flat noise figure semiconductor optical amplifiers," in *European Conference on Optical Communication*, Bordeaux, 2021.

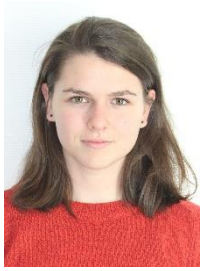

FRANCO Maeva was born in Octobre 1997 in Landerneau (29), France. She obtained an engineer and master degree in 2020 and a doctorate in 2023.
Her PhD research and first Post-doc is a collaboration between Air Liquide Advanced Technologies and the Lab-STICC, UMR CNRS 6285. The focus of the work is on cryogenically cooled semiconductor optical amplifiers. She is now doing a post-doc in CROMA, CNRS UMR 5130, Grenoble, on the theme of noise in infrared detectors.

MOREL Pascal received the M.Eng. and M.Sc. degrees from the Ecole Nationale d'Ingénieurs de Brest, Brest, France, in 2003 and the Ph.D. degree from the Université de Bretagne Occidentale, Brest, France, in 2006.

In 2008, he joined the Ecole Nationale d'Ingénieurs de Brest as an Associate Professor associated to Lab-STICC laboratory (CNRS, UMR 6285) since 2012. Since then, his main field of interest has been in the area of optical communications, mainly focused on semiconductor optical amplifiers modeling, nonlinear impairments and applications. Since 2017, he has been also involved in developing a new research domain named Cryophotonics.

RAMPONE Thierry was born in Cavaillon, France, in 1969. He received the Engineering degree from the École Nationale d'Ingénieurs de Brest, France, in 1992, and the Diplôme d'Études Approfondies (D.E.A.) and the Ph.D. degree from the Université de Bretagne Occidentale, Brest, France, in 1992 and 1997, respectively. His doctoral study principally concerned optical switches based on semiconductor optical amplifiers. In 1998, he joined RESO Laboratory, École Nationale d'Ingénieurs de Brest (ENIB), France, as an Associate Professor. Since January 2012 he is with the Lab-STICC laboratory (UMR CNRS 6285). His research interests include all-optical functions, microwave photonics systems and more recently cryophotonics, mainly based on semiconductor optical amplifiers.

GARDELEIN Arnaud graduated from Polytech'Nantes in 2002. He received a Ph. D. in Electronics from University of Nantes in 2006. In 2007 he worked with CROMA in Chambéry, France in the field of Terahertz Spectroscopy. In 2008 he joined ICFO in Barcelona, Spain, and contributed to a photonic transceiver for quantum key distribution. Since 2011 he works as engineer at Air Liquide advanced Technologies in Sassenage, France. He was involved in the development of electronics for space mechanical cryocoolers. He is currently leading the development of an optical cryocooler prototype for space applications. He also conducts studies on cryophotonics with photonics components at cryogenic temperatures. He has authored and co-authored more than 40 publications.

SHARAIHA Ammar was born in March 1956 in Amman, Jordan. He obtained the master's degree and doctorate from the University of Rennes I, France in 1981 and 1984 respectively and the Habilitation to Direct Research (HDR) from the University of Brest in 2000.

In 1989, he joined the Ecole Nationale d'Ingénieurs de Brest (ENIB) in France as an Associate Professor then as a Full Professor from 2001 to 2024. He was Research Director of ENIB from 2010 to 2014, head of research at ENIB Electronics department and co-head of the research team (70 persons) in the field of Microwaves and Photonics in Lab-STICC, UMR CNRS 6285 from 2010 to 2016 (https://labsticc.fr/fr/annuaire/sharaiha-ammar). Since September 2024, he is Professeur Emerite at ENIB. His main research interests focus on semiconductor optical amplifiers (SOA) for high-speed optical communications systems, Microwave and Photonics (MWP) applications and all-optical signal processing. He has published 200 communications in journal revue, in national and international conferences and holds 5 patents.